extremely flat, meaning disorder is reduced considerably. The conductance deviates by less than 1% over the plateaus, showing that EEL point contacts are of comparable or higher quality than those fabricated by other techniques[4,18,19]. Given that the EEL point contact is short, the width of the plateaus compared to the width of the transitions indicates that lateral confinement is strong[20]. The lower inset of Fig. 4 presents an SGM image to precisely locate the point contact. A unique feature of EEL is the ability to tune a quantum component. In the case of the point contact, additional spots of charge, separated by 10 nm, reliably shift the conductance plots by 1/30 of a plateau period. With the point contact located outside the wire, EEL tuning provides control over geometry while V_p independently controls electron density. Independent control of point contact geometry and electron density is desired to study electron interaction effects in 1D electron systems[19]. We note that a feature near $0.7 \times 2e^2/h$ is often seen when the point contact is drawn inside the wire, but is not seen when the point contact is drawn outside, which may be due to reduced electron density or point contact geometry. An EEL point contact tuned to transmit less than one sub-band has an immediate application as a low-noise charge detector for quantum systems[21].

The device structure is drawn and modified during EEL. The present charge spot area is an order of magnitude larger than the probe to surface contact area[22], so smaller charge spots, and therefore higher EEL resolution, would be attained using a less negative probe bias with a shallower 2DES. A shallow 2DES would further improve resolution, as 2DES lateral depletion would decrease[23]. Lithography and test cycles take several weeks using conventional electron-beam or atomic force microscopy lithography, whereas EEL-drawn components take only a few hours to optimize. EEL is a particularly productive technique where the device geometry is of interest, such as the study of chaotic electron trajectories in large open dots[24], or interaction effects seen in 1D transport[19]. EEL may prove to be particularly useful in the construction of a solid-state scaleable quantum computer, where the required level of uniformity between quantum components is hard to achieve using other schemes[25]. A multifunction scanning probe would visit each component in turn to characterize it, to repair it if necessary, and then to tune it using EEL, so producing the desired array of electrically identical components. A further advantage is that EEL can distance quantum components from surface electrodes, thereby reducing electrical noise and increasing phase coherence times. □

Received 6 March; accepted 18 June 2003; doi:10.1038/nature01841.

1. Beenakker, C. W. J. & van Houten, H. in *Solid State Physics* Vol. 44 (eds Ehrenreich, H. & Turnbull, D.) 1–228 (Academic, New York, 1991).
2. Smith, C. G. Low-dimensional quantum devices. *Rep. Prog. Phys.* **59,** 235–282 (1996).
3. Held, R., Heinzel, T., Studerus, P., Ensslin, K. & Holland, M. Semiconductor quantum point contact fabricated by lithography with an atomic force microscope. *Appl. Phys. Lett.* **71,** 2689–2691 (1997).
4. Curson, N. J. *et al.* Ballistic transport in a GaAs/$Al_xGa_{1-x}As$ one-dimensional channel fabricated using an atomic force microscope. *Appl. Phys. Lett.* **78,** 3466–3468 (2001).
5. vanWees, B. J. *et al.* Quantised conductance of point contacts in a two dimensional electron gas. *Phys. Rev. Lett.* **60,** 848–850 (1988).
6. Wharam, D. A. *et al.* One-dimensional transport and the quantisation of ballistic resistance. *J. Phys. C* **21,** L209–L214 (1988).
7. Eriksson, M. A. *et al.* Cryogenic scanning probe characterization of semiconductor nanostructures. *Appl. Phys. Lett.* **69,** 671–673 (1996).
8. Woodside, M. T. & McEuen, P. L. Scanned probe imaging of single-electron charge states in nanotube quantum dots. *Science* **296,** 1098–1101 (2002).
9. Crook, R. *et al.* Quantum-dot electron occupancy controlled by a charged scanning probe. *Phys. Rev. B* **66,** 121301 (2002).
10. Ihn, T. *et al.* Scanning gate measurements on a quantum wire. *Physica E* **12,** 691–694 (2002).
11. Topinka, M. A. *et al.* Coherent branched flow in a two-dimensional electron gas. *Nature* **410,** 183–186 (2001).
12. Tessmer, S. H., Glicofridis, P. I., Ashoori, R. C., Levitov, L. S. & Melloch, M. R. Subsurface charge accumulation imaging of a quantum Hall liquid. *Nature* **392,** 51–54 (1998).
13. Tortonese, M., Barret, R. C. & Quate, C. F. Atomic resolution with an atomic force microscope using piezoresistive detection. *Appl. Phys. Lett.* **62,** 834–836 (1993).
14. Crook, R., Smith, C. G., Simmons, M. Y. & Ritchie, D. A. Imaging electrostatic microconstrictions in long 1D wires. *Physica E* **12,** 695–698 (2002).
15. Starikov, A. A. *et al.* Effects of accidental microconstriction on the quantized conductance in long wires. Preprint at ⟨arxiv.org/abs/cond-mat/0206013⟩ (2002).
16. Crook, R., Smith, C. G., Simmons, M. Y. & Ritchie, D. A. One-dimensional probability density observed using scanned gate microscopy. *J. Phys. Condens. Matter* **12,** L735–L740 (2000).
17. Williamson, J. G., Timmering, C. E., Harmans, C. J. P. M., Harris, J. J. & Foxon, C. T. Quantum point contact as a local probe of the electrostatic potential contours. *Phys. Rev. B* **42,** R7675–R7678 (1990).
18. Yacoby, A. *et al.* Nonuniversal conductance quantization in quantum wires. *Phys. Rev. Lett.* **77,** 4612–4615 (1996).
19. Thomas, K. J. *et al.* Interaction effects in a one-dimensional constriction. *Phys. Rev. B* **58,** 4846–4852 (1998).
20. Buttiker, M. Quantized transmission of a saddle-point constriction. *Phys. Rev. B* **41,** 7906–7909 (1990).
21. Field, M. *et al.* Measurements of Coulomb blockade with a noninvasive voltage probe. *Phys. Rev. Lett.* **70,** 1311–1314 (1993).
22. Johnson, K. L. *Contact Mechanics* (Cambridge Univ. Press, Cambridge, UK, 1987).
23. Eriksson, M. A. *et al.* Effect of a charged scanned probe microscope tip on a subsurface electron gas. *Superlattices Microstruct.* **20,** 435–440 (1996).
24. Micolich, A. P. *et al.* Evolution of fractal patterns during a classical-quantum transition. *Phys. Rev. Lett.* **87,** 036802 (2001).
25. Bennett, C. H. & DiVincenzo, D. P. Quantum information and computation. *Nature* **404,** 247–255 (2000).

Acknowledgements We thank K. J. Thomas, C. J. B. Ford and M. Kataoka for discussions. A.C.G. fabricated the sample and made the antidot measurements. C.G.S. coordinated the scanning-probe measurement facilities. I.F. and H.E.B. grew the wafer using molecular beam epitaxy (MBE). D.A.R. coordinated the MBE facilities. This work was supported by the EPSRC.

Competing interests statement The authors declare that they have no competing financial interests.

Correspondence and requests for materials should be addressed to C.G.S. (cgs4@cam.ac.uk).

Climate-driven changes to the atmospheric CO_2 sink in the subtropical North Pacific Ocean

John E. Dore, Roger Lukas, Daniel W. Sadler & David M. Karl

Department of Oceanography, School of Ocean and Earth Science and Technology, University of Hawaii, 1000 Pope Road, Honolulu, Hawaii 96822, USA

The oceans represent a significant sink for atmospheric carbon dioxide[1]. Variability in the strength of this sink occurs on interannual timescales, as a result of regional and basin-scale changes in the physical and biological parameters that control the flux of this greenhouse gas into and out of the surface mixed layer[2,3]. Here we analyse a 13-year time series of oceanic carbon dioxide measurements from station ALOHA in the subtropical North Pacific Ocean near Hawaii[4], and find a significant decrease in the strength of the carbon dioxide sink over the period 1989–2001. We show that much of this reduction in sink strength can be attributed to an increase in the partial pressure of surface ocean carbon dioxide caused by excess evaporation and the accompanying concentration of solutes in the water mass. Our results suggest that carbon dioxide uptake by ocean waters can be strongly influenced by changes in regional precipitation and evaporation patterns brought on by climate variability.

The thermodynamic driving potential for the sea-to-air flux of CO_2 is the difference between the partial pressure of the dissolved CO_2 in the surface layer and that of the CO_2 in the overlying air ($\Delta p_{CO_2} = p_{CO_2oce} - p_{CO_2atm}$)[5]. The direction of the flux (F) is governed by the sign of Δp_{CO_2}, while the magnitude is also dependent on the gas exchange coefficient K, which is a parameterized function of wind speed ($F = K\Delta p_{CO_2}$)[5]. Commonly, measurements of dissolved inorganic carbon (DIC) and total alkalinity (TA) in the ocean surface mixed layer are used to calculate p_{CO_2oce}, while p_{CO_2atm} may be obtained from nearby atmospheric sampling stations and corrected for water vapour saturation at *in situ* sea

surface temperature[6]. Beginning in October 1988, the Hawaii Ocean Time-series (HOT) project has collected, on a nearly monthly basis, a suite of physical and biogeochemical data, including surface DIC, TA, temperature, salinity and nutrient measurements, at station ALOHA (22°45′ N, 158° W) in the North Pacific subtropical gyre[4]. We use these data, along with monthly p_{CO_2atm} measurements from the Mauna Loa Observatory (19°32.4′ N, 155°34.8′ W; elevation 3,397 m) and hourly meteorological measurements from the nearby NOAA weather buoy no. 51001 (23°24.1′ N, 162°11.6′ W), to estimate Δp_{CO_2}, K and F from January 1989 to December 2001.

Surface ocean salinity (S), DIC and TA exhibited increasing trends with considerable interannual variability during the study period, while temperature (T) displayed an insignificant ($P > 0.05$) decreasing trend superimposed on a seasonal cycle (Fig. 1). From 1989 to 1992, S averaged 34.94‰. Substantial freshening events occurred in 1995 and 1996, driving S as low as 34.4‰. From mid-1996 to mid-1998, S rose to nearly 35.5‰, and has remained high at around 35.2–35.3‰ through to 2001. The concentrating/diluting effect of salinity changes on DIC and TA can be removed from the data through normalization to a constant S. Following convention, values are normalized to $S = 35$‰ (nDIC = 35DIC/S and nTA = 35TA/S). A strong influence of salinity on the observed trends in DIC and TA is revealed (Fig. 1b, c). The linear increase in nDIC (mean ± s.e.) is 1.19 ± 0.14 μmol kg^{-1} yr^{-1}, 58% less than the trend in DIC of 2.84 ± 0.28 μmol kg^{-1} yr^{-1}; salinity normalization changes both the magnitude and sign of the TA trend, reducing it from 1.62 ± 0.29 to −0.28 ± 0.12 μeq kg^{-1} yr^{-1}.

It is evident from Fig. 1 that while S and nTA display no seasonal patterns, T and nDIC have distinct annual cycles. The cycle of nDIC is sinusoidal, reaching a maximum in April and a minimum in September–October (Fig. 2a). This pattern in surface waters is typical of the North Pacific subtropical gyre, and is largely due to input of DIC from below (via winter mixing) and biological drawdown of CO_2 (via photosynthesis within shallow summer mixed layers)[7]. When we calculate p_{CO_2oce} from DIC and TA data, we also see a seasonal cycle, nearly opposite to that of the nDIC (Fig. 2b). Increasing water temperature raises the partial pressure of dissolved gases; the observed annual cycle of p_{CO_2oce} is largely due to warming in the summer/autumn and cooling in the winter/spring[7]. When p_{CO_2atm} is subtracted from p_{CO_2oce}, the resulting Δp_{CO_2} is negative

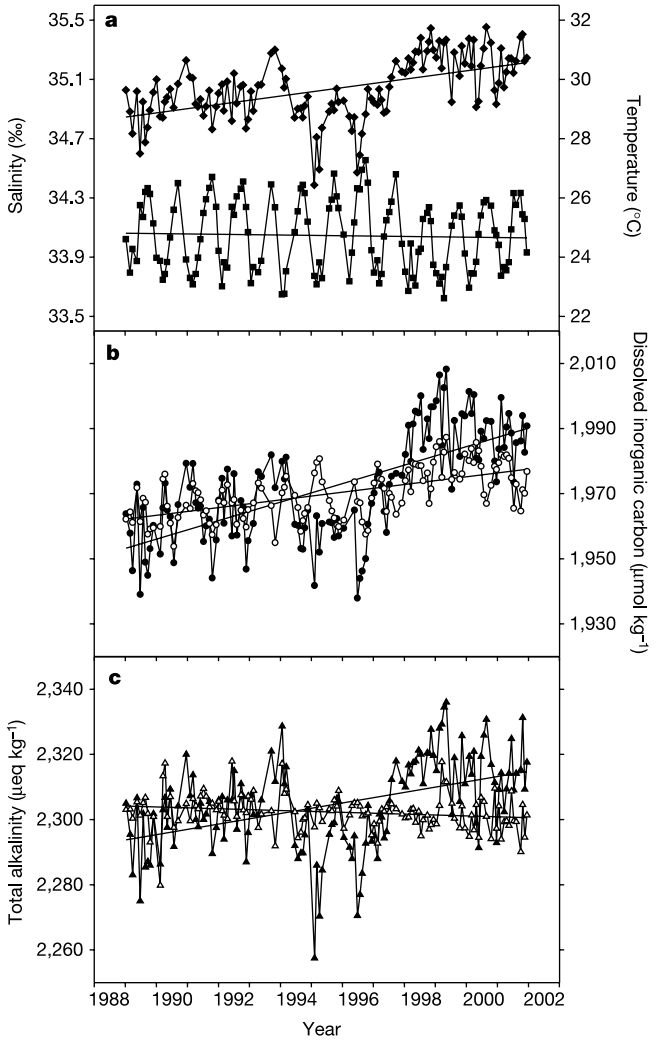

Figure 1 Variability and trends in surface mixed layer salinity (S), temperature (T), dissolved inorganic carbon (DIC) and total alkalinity (TA) at station ALOHA. **a**, Cruise mean values and linear trends in S (diamonds) and T (squares). **b**, Cruise mean values and linear trend in DIC. **c**, Cruise mean values and linear trend in TA. Filled symbols and bold lines indicate *in situ* measurements and trends; open symbols and narrow lines indicate data normalized to a constant salinity of 35‰ and corresponding trends.

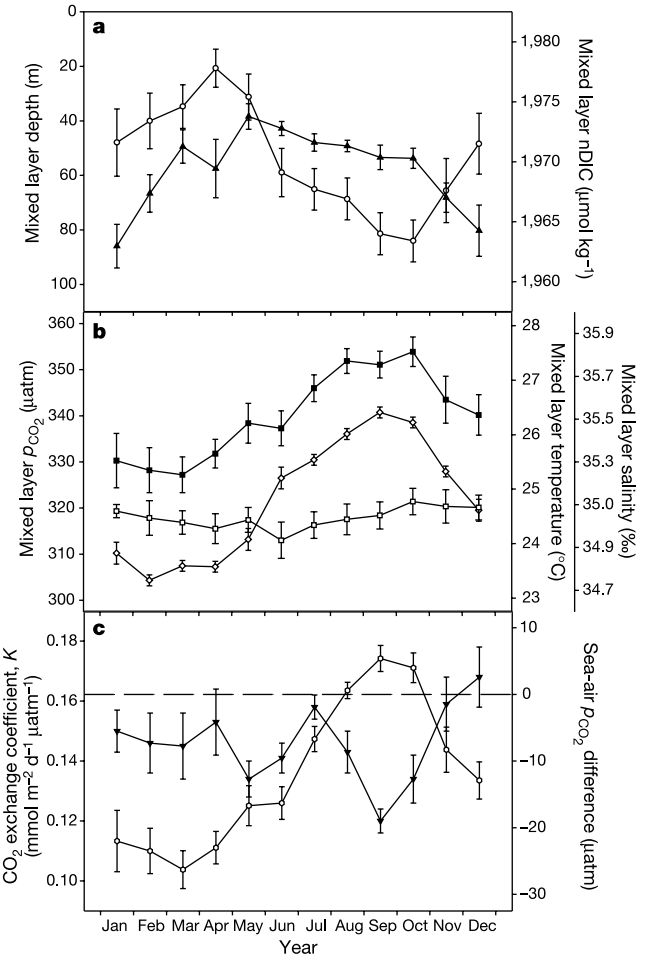

Figure 2 Seasonal patterns in important CO_2 system parameters at station ALOHA, 1989–2001. Symbols and error bars indicate mean values ± one standard error. **a**, DIC normalized to 35‰ salinity (open symbols) and depth of surface mixed layer (filled symbols; determined by 0.125 kg m^{-3} difference in potential density from the surface value). **b**, Mixed layer temperature (open diamonds) and salinity (open squares), and p_{CO_2oce} (filled squares). **c**, Sea–air Δp_{CO_2} (open symbols; horizontal dashed line indicates Δp_{CO_2} of zero) and CO_2 exchange coefficient (filled symbols).

throughout most of the year, indicating a flux of CO_2 into the ocean (Fig. 2c). Only during late summer and early autumn does the flux have the potential to reverse direction; at precisely this time of year, the CO_2 gas exchange coefficient K reaches a minimum owing to low winds (Fig. 2c), thus the annual net CO_2 flux at station ALOHA has been from air to sea during each year of observation.

The concentration of atmospheric CO_2 has been rising for decades owing to anthropogenic CO_2 production, principally from the burning of fossil fuels[8]; this increase amounted to a p_{CO_2atm} trend (mean ± s.e.) of $1.48 \pm 0.05\,\mu atm\,yr^{-1}$ over the period 1989–2001 (Fig. 3a). There has been a corresponding rise in p_{CO_2oce}, yet of a significantly ($P < 0.05$) greater magnitude ($2.46 \pm 0.28\,\mu atm\,yr^{-1}$). Because F depends directly upon Δp_{CO_2}, the difference between the oceanic and atmospheric p_{CO_2} trends results in a significant ($P < 0.001$) reduction with time ($0.15 \pm 0.04\,mmol\,m^{-2}\,d^{-1}\,yr^{-1}$) in the strength of the CO_2 sink (Fig. 3b). Should this reduction continue at this rate, the region would cease to act as a net sink for atmospheric CO_2 by 2008.

We may assess the effect of increasing surface salinity on this suppression of the CO_2 flux as follows. As water is evaporated, solutes are concentrated, hence both DIC and TA rise in direct proportion to salinity. The increasing DIC positively affects p_{CO_2oce}, while the increasing TA has a smaller negative effect. However, determination of the actual increase in p_{CO_2oce} is complicated by the effects of the salinity change on the solubility of CO_2 and on the apparent dissociation coefficients for the carbonic acid system in sea water. Seawater p_{CO_2} rises by about 4.2–4.3% for a 1‰ rise in S over the range of salinities observed at station ALOHA[9]. Thus a rise in salinity from 34.5 to 35.5‰, such as was observed from 1996 to 1998 (Fig. 1a), increases p_{CO_2oce} by about 14–15 μatm. This value is roughly the same as the amplitude of the annual cycle of Δp_{CO_2} (Fig. 2), hence the salinity effect substantially influences the strength of the sea–air CO_2 flux in this region.

Through integration of F over time, we determine that the net annual sea–air flux of CO_2 at station ALOHA between 1989 and 2001 varied from -1.02 to $-0.17\,mol\,m^{-2}$ (Fig. 4a). When we recalculate the p_{CO_2oce} data from Fig. 3 while holding S constant at 34.94‰ (the initial 1989–92 mean), it becomes evident that the CO_2 sink was strongly affected by salinity, particularly from 1996 to 2001 (Fig. 4a). Annual CO_2 fluxes were suppressed by as much as $0.29\,mol\,m^{-2}$ relative to a constant-salinity scenario (Fig. 4b). If the effects of changing salinity are removed from the data, 40% of the observed 13-yr trend in F disappears. The remaining trend of $0.09 \pm 0.04\,mmol\,m^{-2}\,d^{-1}\,yr^{-1}$ is still significant ($P < 0.05$), and

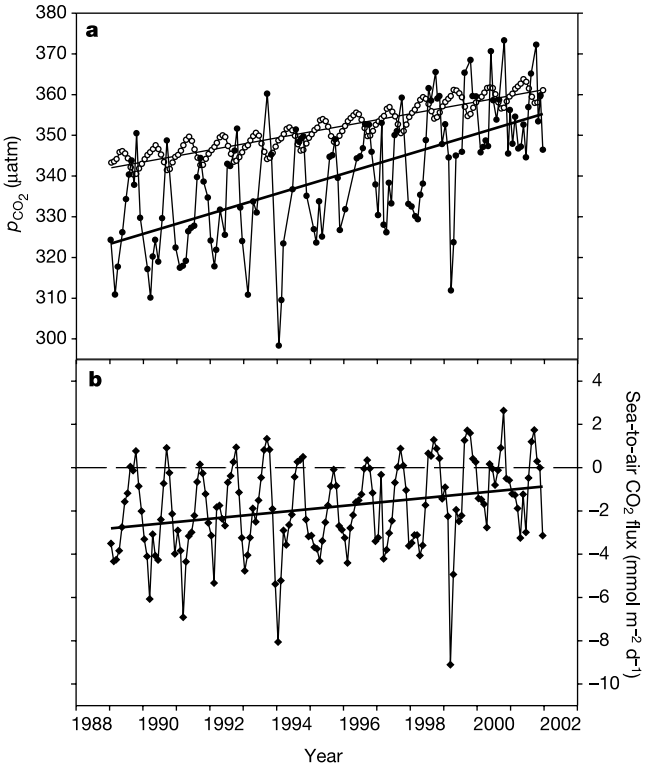

Figure 3 Interannual variability and trends in p_{CO_2atm}, p_{CO_2oce} and the sea–air flux of CO_2 at station ALOHA. **a**, Cruise mean values and linear trend in p_{CO_2}. Filled symbols and solid line indicate ocean mixed layer p_{CO_2} measurements and trend; open symbols and narrow line indicate atmospheric data corrected for water saturation and corresponding trend. **b**, Monthly flux of CO_2 from ocean to atmosphere. Values of p_{CO_2oce} were interpolated to the fifteenth day of each month to facilitate calculation of monthly F. Solid line indicates linear trend in flux.

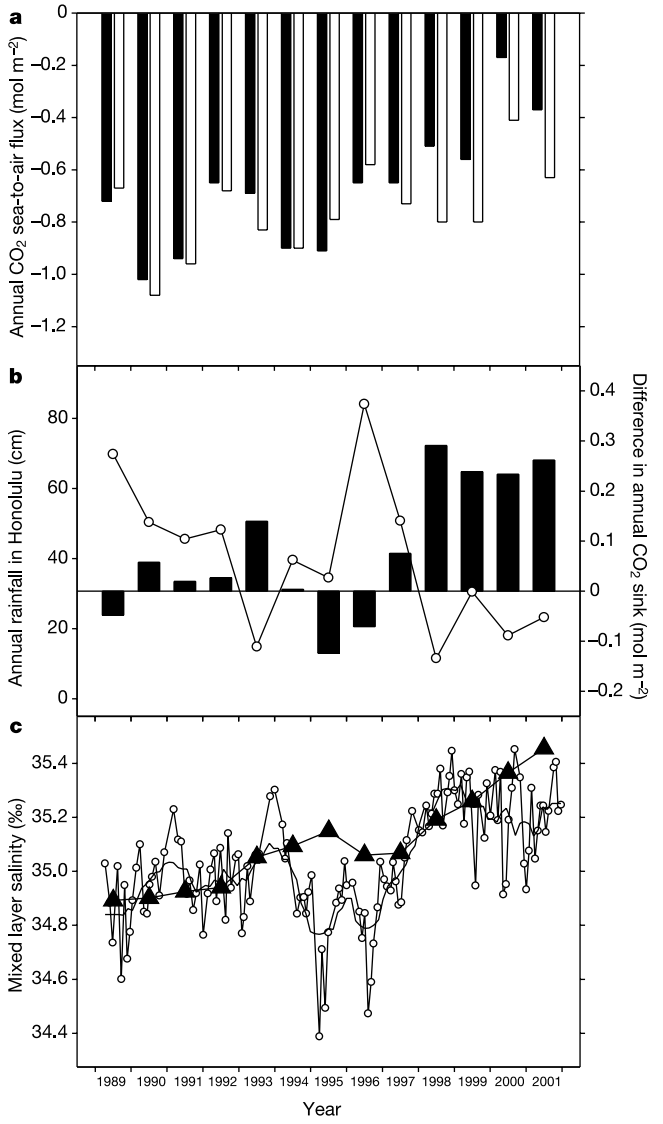

Figure 4 Salinity effect on annual net sea–air fluxes of CO_2 at station ALOHA. **a**, Measured fluxes (filled bars) and fluxes predicted at a constant salinity of 34.94‰ (open bars). **b**, Reduction in CO_2 flux attributable to salinity effect (filled bars) and total annual rainfall at Honolulu International Airport (open symbols). **c**, Mixed layer salinity (open symbols) and its annual running mean (bold curve), and salinity predicted (solid symbols) by simple rainfall model (see text).

may be due to the effects of interannual variations in mixing, advection or biological processes. For example, the observed decreasing trend in nTA (Fig. 1c) contributes to rising p_{CO_2oce}, and may indicate long-term changes in the rates of biological calcification and/or calcite export and dissolution. Because T displays no rising temporal trend (Fig. 1a), temperature variations cannot be invoked to account for the remaining decrease in sink strength.

When the magnitude of the salinity effect and the annual rainfall at Honolulu International Airport (21°18′ N, 157°54′ W) are compared, a correspondence between low rainfall and suppression of the CO_2 sink is suggested (Fig. 4b). Our shipboard sampling gives us only snapshots in time; the measured salinity on any particular cruise will be affected strongly by the recent history of rainfall and mixed layer depth. However, we can roughly estimate the effect of rainfall deficits on surface salinity as follows. First, we assume that the deepest mixed layers observed (~120 m) occur at some time during each winter, and that the annual rainfall at Honolulu is indicative of the rainfall mixed to that depth at station ALOHA. Second, we assume that evaporation and precipitation were roughly in balance over the initial 1989–92 time period, and that evaporation remained constant thereafter (53.53 cm yr^{-1}). Although the rainfall at station ALOHA may not always track that in Honolulu, and although variations in evaporation, turbulent salt flux and water mass advection must be considered for a rigorous salt budget, the results of this exercise suggest that a net freshwater loss from the ocean due to the observed rainfall deficit is sufficient to account for the magnitude of the observed salinity increase (Fig. 4c).

We have shown that rising salinity in the subtropical North Pacific Ocean near Hawaii from 1989 to 2001, substantially influenced by recent rainfall deficits, has directly caused a reduction in the strength of the CO_2 sink. Most of this salinity increase occurred over a two-year period (1996–98), hence we may be observing a manifestation of a climate oscillation or regime shift, rather than a long-term temporal trend. Drought conditions over a large area of the North Pacific have persisted since the mid-1990s[10–12], and may be related to both the El Niño and Pacific Decadal Oscillation climate phenomena[11–13]. In addition, recent biogeochemical and fisheries data suggest a biological response to a potential late-1990s shift in North Pacific climate[14,15]. As the ocean CO_2 time-series data records lengthen, our ability to draw direct links between specific climate phenomena and interannual to decadal variability in the oceanic carbon cycle will improve. Regional changes in evaporation and precipitation patterns accompanying climate variability have the potential to significantly alter the global ocean sink for CO_2, and should be considered when modelling the ocean carbon cycle. Moreover, there is reason to be concerned about the influence of hydrologic changes on the response of the oceanic CO_2 sink to anthropogenic climate change. □

Methods

Sampling and analyses

Shipboard sampling was conducted within a six-nautical-mile radius of the nominal position of station ALOHA. Discrete water samples were collected using a rosette system fitted with a SeaBird CTD (conductivity, temperature, depth) sensor for continuous salinity and temperature determinations. Samples for DIC and TA were returned to our shore-based laboratory, and analysed using semi-automated coulometry and open-cell titration techniques, respectively, following the recommendations of the DOE[16] with minor modifications. The accuracy of these measurements was maintained using certified seawater reference materials[17]. Calculations of p_{CO_2oce} were carried out[18], using independently validated[19,20] parameterizations of the apparent dissociation constants for carbonic acid in sea water[21] that were subsequently refitted[22].

Supporting data sets

Monthly atmospheric CO_2 mole fractions measured at the Mauna Loa Observatory[23] were obtained from the Carbon Dioxide Information Analysis Center (http://cdiac.ornl.gov/ftp/maunaloa-co2/maunaloa.co2). Monthly rainfall data from Honolulu International Airport were obtained from the National Weather Service Pacific Regional Headquarters (http://www.prh.noaa.gov/hnl/climate/PHNL_rainfall.html). Hourly measurements of sea surface temperature and wind speed from weather buoy no. 51001 were obtained from the National Weather Service National Data Buoy Center (http://seaboard.ndbc.noaa.gov/station_history.phtml?$station = 51001). These meteorological data sets have been shown to be well correlated with discrete observations made at station ALOHA during HOT cruises[24]. Hourly buoy data was used to calculate K (ref. 5), which was then binned by month.

Treatment of missing data

The HOT programme obtained measurements of mixed layer DIC and TA on 122 and 118 of the 131 cruises completed during 1989–2001, respectively. Several additional data points during 1989–90 were obtained from parallel measurements[25] made on samples collected during HOT cruises using similar methods and identical reference materials. On a single cruise (HOT-4; February 1989), a DIC measurement was available, but an average value of 2,303.2 μeq kg^{-1} was assumed for nTA. In all, p_{CO_2oce} was calculated for 125 occupations of station ALOHA between 1989 and 2001. Several short gaps in the buoy data sets were filled using the monthly averaged values from the entire 13-yr record.

Received 17 February; accepted 3 July 2003; doi:10.1038/nature01885.

1. Siegenthaler, U. & Sarmiento, J. L. Atmospheric carbon dioxide and the ocean. *Nature* **365,** 119–125 (1993).
2. Bates, N. R., Pequignet, A. C., Johnson, R. J. & Gruber, N. A short-term sink for atmospheric CO_2 in subtropical mode water of the North Atlantic Ocean. *Nature* **420,** 489–493 (2002).
3. Gruber, N., Keeling, C. D. & Bates, N. R. Interannual variability in the North Atlantic Ocean carbon sink. *Science* **298,** 2374–2378 (2002).
4. Karl, D. M. & Lukas, R. The Hawaii Ocean Time-series (HOT) program: Background, rationale and field implementation. *Deep-Sea Res. II* **43,** 129–156 (1996).
5. Wanninkhof, R. Relationship between wind speed and gas exchange over the ocean. *J. Geophys. Res.* **97,** 7373–7382 (1992).
6. Winn, C. D., Mackenzie, F. T., Carrillo, C. J., Sabine, C. L. & Karl, D. M. Air-sea carbon dioxide exchange in the North Pacific Subtropical Gyre: Implications for the global carbon budget. *Glob. Biogeochem. Cycles* **8,** 157–163 (1994).
7. Ishii, M. *et al.* Seasonal variation in total inorganic carbon and its controlling processes in surface waters of the western North Pacific subtropical gyre. *Mar. Chem.* **75,** 17–32 (2001).
8. Houghton, J. T., Jenkins, G. J. & Ephraums, J. J. (eds) *Climate Change: The IPCC Scientific Assessment* (Cambridge Univ. Press, Cambridge, UK, 1990).
9. Weiss, R. F., Jahnke, R. A. & Keeling, C. D. Seasonal effects of temperature and salinity on the partial pressure of CO_2 in seawater. *Nature* **300,** 511–513 (1982).
10. Waple, A. M. *et al.* Climate assessment for 2001. *Bull. Am. Meteorol. Soc.* **83,** S1–S62 (2002).
11. Minobe, S. & Nakanowatari, T. Global structure of bidecadal precipitation variability in boreal winter. *Geophys. Res. Lett.* **29,** 1396–1399 (2002).
12. Lukas, R. Freshening of the upper thermocline in the North Pacific subtropical gyre associated with decadal changes in rainfall. *Geophys. Res. Lett.* **28,** 3485–3488 (2001).
13. Hoerling, M. & Kumar, A. The perfect ocean for drought. *Science* **299,** 691–694 (2003).
14. Dore, J. E., Brum, J. R., Tupas, L. M. & Karl, D. M. Seasonal and interannual variability in sources of nitrogen supporting export in the oligotrophic subtropical North Pacific Ocean. *Limnol. Oceanogr.* **47,** 1595–1607 (2002).
15. Chavez, F. P., Ryan, J., Lluch-Cota, S. E. & Ñiquen, M. C. From anchovies to sardines and back: Multidecadal change in the Pacific Ocean. *Science* **299,** 217–221 (2003).
16. DOE *Handbook of Methods for the Analysis of the Various Parameters of the Carbon Dioxide System in Sea Water* Version 2 (eds Dickson, A. G. & Goyet, C.) ORNL/CDIAC-74 (Carbon Dioxide Information Analysis Center, Oak Ridge National Laboratory, US Department of Energy, Oak Ridge, Tennessee, 1994).
17. Dickson, A. G. Reference materials for oceanic CO_2 measurements. *Oceanography* **14,** 21–22 (2001).
18. Lewis, E. & Wallace, D. W. R. *Program Developed for CO_2 System Calculations* ORNL/CDIAC-105 (Carbon Dioxide Information Analysis Center, Oak Ridge National Laboratory, US Department of Energy, Oak Ridge, Tennessee, 1998).
19. Lueker, T. J., Dickson, A. G. & Keeling, C. D. Ocean p_{CO_2} calculated from dissolved inorganic carbon, alkalinity, and equations for K_1 and K_2: Validation based on laboratory measurements of CO_2 in gas and seawater at equilibrium. *Mar. Chem.* **70,** 105–119 (2000).
20. Lee, K., Millero, F. J., Byrne, R. H., Feely, R. A. & Wanninkhof, R. The recommended dissociation constants for carbonic acid in seawater. *Geophys. Res. Lett.* **27,** 229–232 (2000).
21. Merbach, C., Culberson, C. H., Hawley, J. E. & Pytkowicz, R. M. Measurement of the apparent dissociation constants of carbonic acid in seawater at atmospheric pressure. *Limnol. Oceanogr.* **18,** 897–907 (1973).
22. Dickson, A. G. & Millero, F. J. A comparison of the equilibrium constants for the dissociation of carbonic acid in seawater media. *Deep-Sea Res.* **34,** 1733–1743 (1987).
23. Keeling, C. D. & Whorf, T. P. in *Trends: A Compendium of Data on Global Change* (Carbon Dioxide Information Analysis Center, Oak Ridge National Laboratory, US Department of Energy, Oak Ridge, Tennessee, 2002).
24. Tupas, L., *et al. Hawaii Ocean Time-series Data Report 4: 1992* (SOEST Technical Report 93-14, Univ, Hawaii, 1993).
25. Keeling, C. D. in *The Global Carbon Cycle* (ed. Heimann, M.) 413–429 (NATO ASI Series, Vol. I15, Springer, Berlin, 1993).

Acknowledgements We thank past and present HOT programme scientists and staff, seagoing support personnel and the crews of the many research vessels used to collect these data. We also thank the National Oceanic and Atmospheric Administration and the Department of Energy for access to critical meteorological and atmospheric CO_2 data sets. This work was supported by the National Science Foundation.

Competing interests statement The authors declare that they have no competing financial interests.

Correspondence and requests for materials should be addressed to J.E.D. (jdore@hawaii.edu).